Knocking on surfaces : interactions of hyperthermal particles with metal surfaces

Ueta, H.

Citation

Ueta, H. (2010, November 16). *Knocking on surfaces : interactions of hyperthermal particles with metal surfaces*. Retrieved from https://hdl.handle.net/1887/16153

Chapter 5

Scattering of Hyperthermal Nitrogen Atoms from the Ag(111) Surface

Measurements on scattering of hyperthermal N atoms from the Ag(111) surface at temperatures of 500, 600 and 730 K are presented. The scattered atoms have a two-component angular distribution. One of the N components is very broad. In contrast, scattered Ar atoms exhibit only a sharp, single-component angular distribution. There are noteworthy features in the angle-resolved energy of the scattered N when compared with Ar. Taking into account the relative masses involved, N atoms lose significantly more energy at the surface than Ar. However, there is a preferentially loss mechanism that predominantly affects low-energy N atoms with small total scattering angle trajectories. The results are interpreted in terms of probing of different interaction potentials: strongly attractive and almost purely repulsive, and spin-state changes during the interaction of N with the surface appear probable.

5.1 Introduction

Knowledge of gas-surface interaction dynamics is important for the development of a detailed understanding of a range of processes involved in sputtering, plasma etching (including fusion reactor wall erosion [1, 2]) and heterogeneous catalytic reactions. This motivates the study of atom and molecule scattering from surfaces for a wide variety of systems [3-6]. In general, scattering is characterised by correlating the angular and energy distributions of scattered particles with controllable parameters such as the incidence angle and energy, the surface temperature, and the surface structure and state (e.g., clean/precovered; ordered/disordered; etc.).

For noble gas atoms only a physisorption interaction is known, involving a shallow well and a repulsive wall that is located relatively far from the surface. When the kinetic energy with which such atoms impinge on a surface increases, they probe deeper into the wall, but the interaction remains purely repulsive. For reactive atoms and molecules the situation is more complex due to the additional possibility of chemisorption interactions. For dissociative adsorption of molecules, an activation barrier may exist due to the necessity of bond-breaking prior to adsorption. Depending on the system, molecules can stick at the surface provided they have sufficient energy to overcome the activation barrier. Reactive atoms (produced by predissociation of molecules) can access the chemisorption well directly without having to overcome such a barrier. Nonadiabatic effects such as spin-state changes, electron transfer, and electron-hole pair excitations may also play a significant role in the scattering processes [7, 8].

To date, extensive studies involving the interactions of hyperthermal noble gas atoms with metal [9-20], semiconductor [9, 21], and graphite [22-24] surfaces, and with self-assembled monolayers [25], have been performed. In contrast, scattering of reactive atoms (at thermal and/or hyperthermal energies) has been reported from only a relatively limited number of surfaces (some examples are H(D)/graphite [26], H/KCl(001) [27], F/Fluorinated Si surface [28-30], and O and Cl/hydrocarbon surface [31-35].). In this paper, we deal with the scattering of N atoms from Ag(111). N_2 is known to be very inert toward Ag(111) [36, 37]. Recombinative desorption of N_2 from the N precovered Ag surface was studied by Carter *et al.* [36]. The precovered surfaces in that study were prepared by irradiation with a low-density N_2 microwave discharge that produced N atoms directly. The angular distribution of desorbing N_2 was sharply peaked along the surface normal (the distribution could be fitted with a $\cos^{75}\theta_d$ function). Rotationally and/or vibrationally excited N_2 desorption was indicated based on the absence of $N_2(v=0,1)$ states.

Although there have been no reports of N_2 dissociation on Ag(111) by experimental or theoretical studies, dissociation on Cu(111) and Au(111) surfaces was reported by Wang *et al.* based on DFT calculations [38]. Dissociation of N_2 on Au(111) (barrier height ~6.5 eV) is more difficult than on Cu(111) (barrier height ~3.75 eV). By analogy to the Au(111) results, dissociation of N_2 on Ag(111) would also be expected to have a high activation barrier. Wang *et al.* also calculated the adsorption energy of the N atom on Cu, Ag, and Au(111) surfaces as a function of adsorption site. They found the fcc hollow site to be the most stable adsorption site. A comparative study of some open-shell systems, including N atoms, on the Ag(111) surface has been carried out by Kokh *et al.* using the embedded cluster and multireference single- and double-excitation configuration interaction (MRD-CI) methods [39]. They computed potential energy curves of ground and excited states N atoms interacting with Ag_{91} clusters.

In the current study, energetic N atoms are generated using a cascaded arc source [40, 41]. The mixed N and N_2 beams produced are scattered from a Ag(111) surface. In this paper we focus on the angular and energy distributions of the scattered N atoms. For comparison purposes, results for scattering of Ar with comparable energies are also shown. Clear differences between the two atoms are evident in the measured distributions. The features observed may be due to differences between the interaction of ground- and excited-state N atoms in the beam with the surface. The results are interpreted in terms of the N atoms interacting with a more corrugated surface potential, consistent with probing of the chemisorption well.

5.2 Experimental

The experiments were performed in an ultrahigh vacuum apparatus with a triply differentially pumped plasma source. This machine was previously used in combination with a supersonic molecular beam source [42]. A cascade arc plasma source has been mounted in place of the molecular beam source. The modified setup has been described elsewhere [43]. Details specific to the current configuration are outlined below.

The first stage of the beam line contained the cascaded arc source [40, 41, 44, 45]. This produced a wall-stabilised high-density linear plasma. Plasma was initiated by discharge at three symmetrically mounted cathode tips (field-emitting type) and was transported through a channel in a stack of 5 floating, mutually isolated copper plates (plate thickness of 5 mm). The plasma channel had a diameter (∅*)* of 2.5 mm. Plasmas were run with a constant current through the arc of ~60 A (20A; ~150V/tip for pure N_2 plasma, and 20A; ~88V/tip for pure Ar plasma). The plasma expanded into the first stage of the beamline, which was pumped by a 1284 m^3/h roots pump (base pressure ~4×10^{-4} mbar). During N_2 plasma operation, the stagnation pressure in the gas line was maintained at 320 mbar. This caused the pressure in the first stage to rise to approximately 1.1×10^{-1} mbar.

Particles entered the second stage of the beamline (base pressure ~5×10^{-6} mbar) through a homemade conical skimmer with a ∅=0.5 mm opening. The distance between the nozzle of the cascaded arc and the skimmer was ~1.75 cm. This stage was pumped by a 500 L/s turbo molecular pump (TMP). It contained a beam flag, a mechanical chopper wheel and a pair of deflection plates that were used to remove charged particles from the beam. During N_2 plasma operation, the pressure in this stage was approximately 3.5×10^{-5} mbar.

The beam entered the third (buffer) stage (base pressure ~2×10^{-8} mbar; pumped by a 330 L/s TMP) through a skimmer (Beam Dynamics Inc.) with a ∅=1 mm opening, before finally reaching the scattering chamber. The sample was mounted in the centre of this chamber on a three-axis goniometer (described in detail elsewhere [46]). This section contains an ion sputter gun and a differentially pumped quadrupole mass spectrometer (QMS, Extrel, type MEXM060 2.9C/4P8). This QMS could be rotated in a horizontal plane around the sample. It was used for measuring the in-plane angular distribution of scattered particles, for time-of-flight (TOF) measurements (in combination with the chopper), and for postirradiation temperature programmed desorption (TPD) measurements. Particles entered the QMS through an aperture with ∅=3 mm. The consequent detector acceptance angle was ~1.6° (assuming a point source at the sample position). The scattering chamber and the QMS were pumped by a 520 L/s TMP and a 210 L/s TMP, respectively. The base pressures were 3×10^{-10} mbar and 2×10^{-10} mbar, respectively. During TOF measurements, the pressure in the scattering chamber increased to ~6×10^{-10} mbar.

The Ag crystal used was oriented to within 0.1° of the (111) face. The surface was cleaned by repeated cycles of Ar^+ sputtering, followed by annealing to 800 K for several minutes. The surface temperature (T_S) was monitored with a K-type thermocouple inserted into a hole in the side of the crystal. The surface structure was verified by low-energy electron diffraction. In addition, N_2 TPD spectra from the N-covered Ag(111) surface (prepared by N beam irradiation at T_S=300 K) were in agreement with those previously reported [36].

The sample could be moved aside, allowing direct measurement of the incident beam. The full width at half maximum (FWHM) of the direct beams was ~1.6°. For this study, beam from pure nitrogen and argon plasmas were used. When nitrogen was used as the feed gas, the resultant beam consisted of a mixture of N and N_2. The QMS ratio of N:N_2 measured in the direct beam was ~1:1 (not corrected for the N_2 cracking contribution to N). The beam may have contained not only ground state N(^{4}S) and $N_2(X^1\,\Sigma_g^+)$ but also electronically excited N(^{2}D) and N(^{2}P) and $N_2(A^3\,\Sigma_u^+)$. By changing the electron impact energy of the QMS ionizer (appearance potential measurements), we detected N at energies below the threshold of the ground state. Although the relative composition of the different states has not been quantified, the beam clearly did contain electronically excited N atoms. In contrast, excited state N_2 was not detected in the beam.

In other studies involving N atoms, which were produced under a variety of discharge conditions, the respectively fractions of ^{2}D and ^{2}P metastable atoms were determined as 0.17 and 0.06 [47], 0.04 and 0.013 [48], and 0.3 and 0.1 [49] relative to the ^{4}S ground state N. Very high concentrations of ^{2}D and ^{2}P (~70% and ~30%) were reported by Brunetti *et al.* using a microwave discharge [50]. The ^{4}S component was estimated as not greater than 10%. The high metastable content was attributed to sampling inside the discharge core and to the absence of wall effects in the instrument. In addition, a He-N_2 gas mixture was used, which increases the metastable concentrations. In contrast, for cascaded arc produced plasmas there are several mechanisms by which N metastable can be quenched to the ground state [41]. Wall effects can have a big influence in the channel and nozzle regions. As a result we believe that the ^4S state was the dominant component in our beam, similar to most previous studies.

TOF spectroscopy was used to determine the kinetic energy of the incident particles. The raw data was corrected for the trigger delay and for the flight times of ions through the QMS. The trigger delay originates primarily from a small physical misalignment between the trigger sensor and the beam-open position of the chopper. This delay is a linear function of the inverse of the chopper frequency. It was determined by measuring the TOF of an Ar beam at several different chopper frequencies. Ion flight times in the QMS were estimated on the basis of simulations using the SIMION code. The particle beams had hyperthermal energies (range from 4 to 7 eV). As a consequence, the neutral particle flight time and the QMS ion flight time were on the same order of magnitude in our apparatus (55-70 μs and 25-30 μs respectively). Failure to account for the ion flight time correctly would result in a substantial systematic error. TOF experiments were performed using a 0.5% duty-cycle chopped beam. The N TOF spectra were corrected for the QMS-induced contribution from N_2 cracking by subtraction of the cracking-factor-corrected N_2 TOF intensity (see below). Scattered intensities were expressed as a fraction of the incident beam intensity. The incident energy, final energies at different scattering angles, and the angular distributions were derived from TOF measurements after fitting by a single shifted Maxwell-Boltzmann distribution convoluted over the finite chopper opening time and over the spread of arrival times of particles at the surface [42, 51, 52].

In the current study, incident beams of N with average energy ($\langle E_i \rangle$) of ~4.3 eV and of Ar with $\langle E_i \rangle$~6.6 eV were used. Note that our beams had a broad energy distribution (FWHM ~5.0 and ~6.2 eV respectively). Since we have no velocity selector, we did not have the well-defined monoenergetic beams that are typical of supersonic molecular beam studies. In this study, the N_2 cracking factor for the incident (scattered) N beams was determined on the basis of matching the tail of the incident (scattered) N TOF spectra and that of the slower incident (scattered) N_2 TOF spectra. Note that this method represents an upper-limit of the cracking factor, potentially overestimating the contribution due to N_2. The trends in the intensity and energy distributions shown in the next section are independent of the cracking factor used, although the absolute values change if a smaller factor is employed.

5.3 Results and Discussion

In this study, we focus on N atoms scattering from the clean Ag(111) surface. N atoms can stick to the surface at room temperature. They will desorb, via recombination to N_2, at T_S<500 K [36, 53]. All data presented in this text was collected for $T_S \geq 500$ K. Since this is above the recombinative desorption temperature, the standing coverage of atomic N during measurements remains low and we are

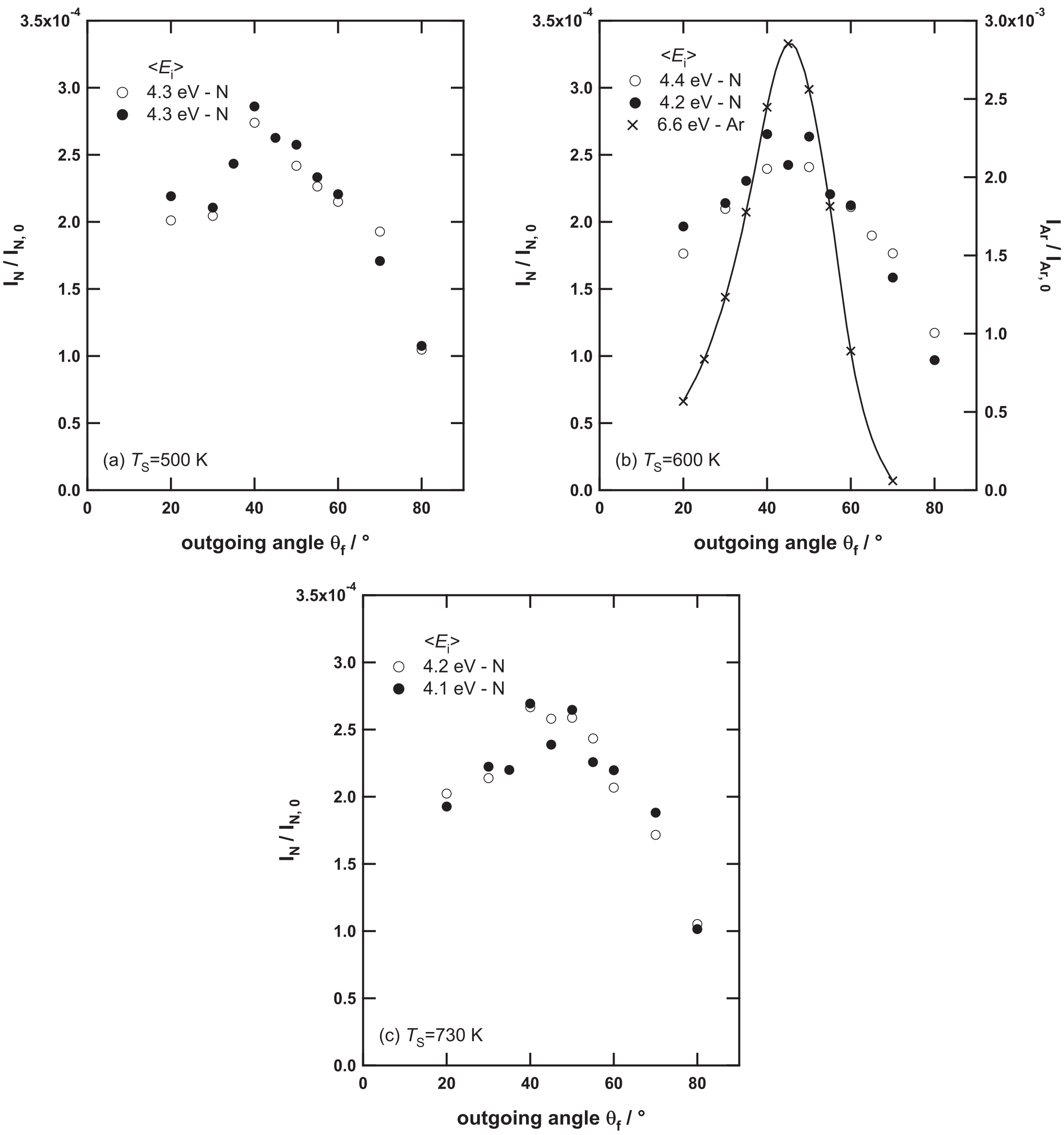

Figure 5. 1 Angle-resolved density distributions of N atoms ($<E_i>$~4.3 eV; open and filled circles) and Ar atoms ($<E_i>$~6.6 eV; crosses) scattered from Ag(111) at θ_i=40°. The panels show (a) N, T_S=500 K; (b) N and Ar, T_S=600 K; and (c) N, T_S=730 K. The scattered Ar intensities in (b) are indicated on the right ordinate. The scattered intensities are normalised to the intensity of the corresponding direct beam. For all three surface temperatures, two independent data set are plotted for the N density distributions. The line connecting the Ar points is intended to guide the eye.

working with a quasi-clean (N atom free) surface. Postirradiation TPD confirmed that there was no significant retention of N by the surface. N atom scattering results are shown for surface temperatures of 500, 600 and 730 K. Results for Ar scattering at T_S=600 K are included for comparison purposes.

We begin by presenting angular distributions of scattered N and Ar in figure 5.1. The incidence angle (θ_i) was 40° (measured with respect to the surface normal). All data points were derived from individual TOF measurements after the corrections outlined in the experimental section. Figure 5.1(a-c) shows the angular distributions of

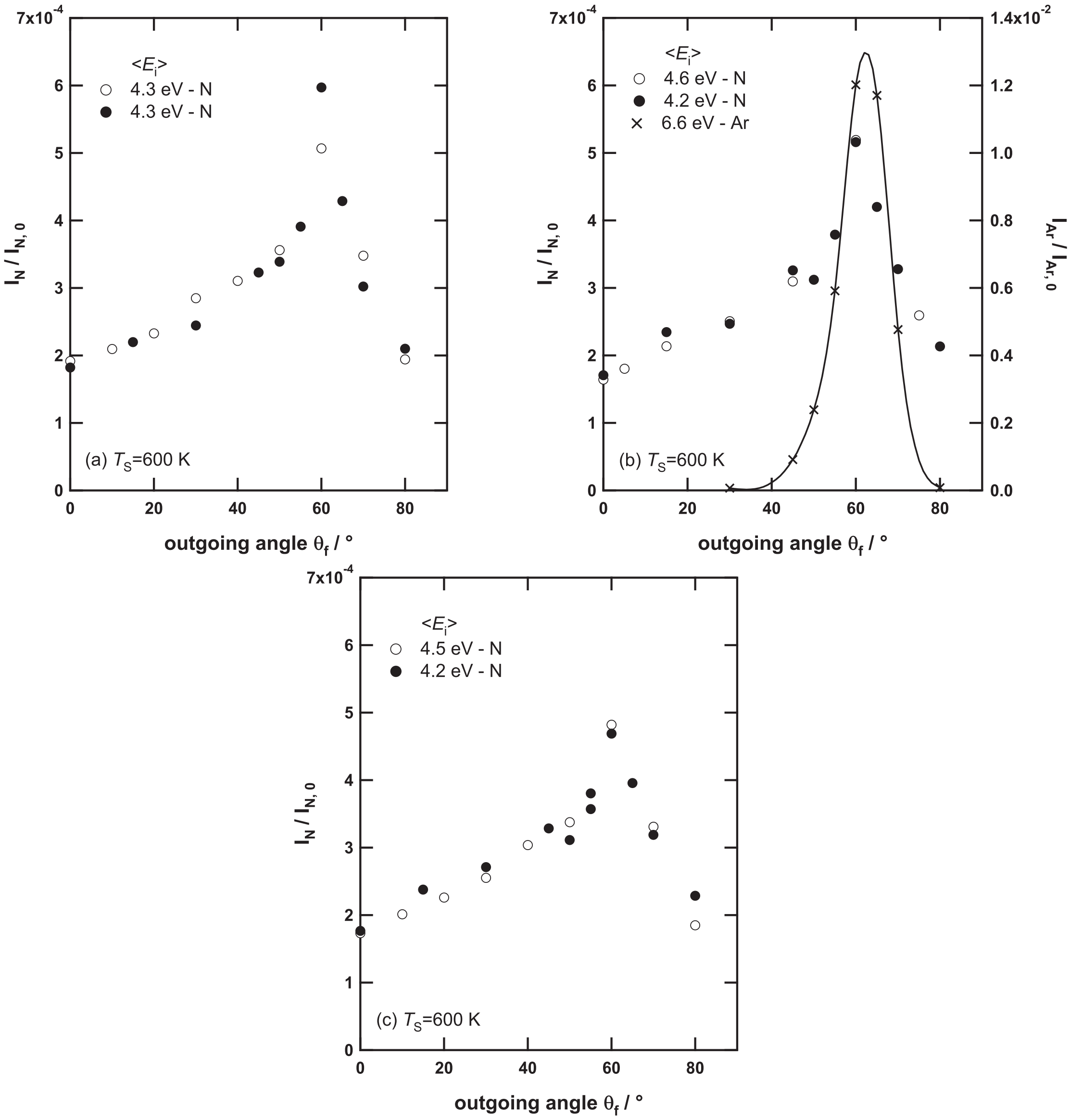

Figure 5. 2 Angle-resolved density distributions of N atoms ($<E_i>$~4.3 eV; open and filled circles) and Ar atoms ($<E_i>$~6.6 eV; crosses) scattered from Ag(111) at θ_i=60°. The panels show (a) N, T_S=500 K; (b) N and Ar, T_S=600 K; and (c) N, T_S=730 K. The scattered Ar intensities in (b) are indicated on the right ordinate. The scattered intensities are normalised to the intensity of the corresponding direct beam. For all three surface temperatures, two independent data set are plotted for the N density distributions. The line connecting the Ar points is intended to guide the eye.

N scattered from the Ag(111) surface at T_S=500, 600 and 730 K. Ar scattering from the clean surface at T_S=600 K is included on figure 5.1(b). The intensity values shown represent fractions of the corresponding incident beam intensities. Note that the maximum intensity of the Ar distribution (right ordinate) is approximately 10 times larger than that of the N distribution (left ordinate), plotted using the same relative units.

The Ar scattering distribution has a relatively sharp peak that is slightly offset from the specular angle (peak maximum ~45º). The FWHM of the Ar distribution is approximately 25° (QMS angular acceptance is ~1.6°). This value is broader than results previously reported for E_i of 0.5-2.6 eV [15, 17]. It continues a trend of increasing angular width with increasing energy that was already evident in the highest energy measurements of the previous work [17] and it is also in agreement with the results of molecular dynamics simulations [15]. The trend is consistent with Ar probing the repulsive potential wall more deeply (structure scattering).

In contrast, N scattering yields very broad angular distributions. Significant scattered intensity is evident even at small (θ_f=20°) and very large (θ_f=80°) outgoing angles, whereas Ar scattering shows relatively little or no scattered intensity at these angles. There is an indication of a surface-temperature dependence in the N angular distributions. At T_S=600 K and 730 K the distributions appear to consist of a single broad component, centred approximately on the specular angle. In contrast, the distribution for T_S=500 K may contain two components. The shape suggests that a second, sharper component is superimposed on the broad distribution. It is possible that two components are present in all three N distributions, but that the relative contribution changes such that the sharper component becomes less evident as the surface temperatures is increased.

Equivalent results for N and Ar scattering at θ_i=60° are shown in figure 5.2(a-c). As before, the N and Ar (T_S=600 K only) intensities are indicated on the left and right ordinates respectively. At this incidence angle, the ratio between the maximum N and Ar intensities has increased to a factor of approximately 20. As was the case for θ_i=40°, the Ar distribution is sharp with a maximum at a slightly off-specular direction (θ_f~62°). In contrast, all of the N atom distributions now exhibit a sharp peak superimposed on a broader background. This is confirmation of the two-component distribution that was suggested by the results obtained at θ_i=40°. At θ_i=60°, the measurements for all three surface temperatures clearly contain two components. The broad component is similar to that observed in figure 5.1. The additional sharp component is close to the specular position and is reminiscent of the Ar distribution. The maximum intensity (primarily determined by the intensity of the sharp component) appears to decrease somewhat with increasing surface temperature. It is the sharp peak that is most affected; the shape and intensity of the broad component does not appear to be significantly altered by increasing the surface temperature.

It should be noted at this point that the angular distributions of scattered N_2 (not shown) are similar in shape to those of scattered Ar. Consequently, failure to fully remove the contribution from N_2 cracking would invariably lead to a sharp peak around the specular position. It is for this reason that, as mentioned in the experimental section, we adopted a correction procedure that maximised the estimation of the N_2 cracking contribution to the measured N distribution. As a result, we are confident that the sharp features evident in figure 5.1 and 5.2 are due solely to N atom scattering. Indeed, there is a strong possibility that we have underestimated the intensity of these peaks.

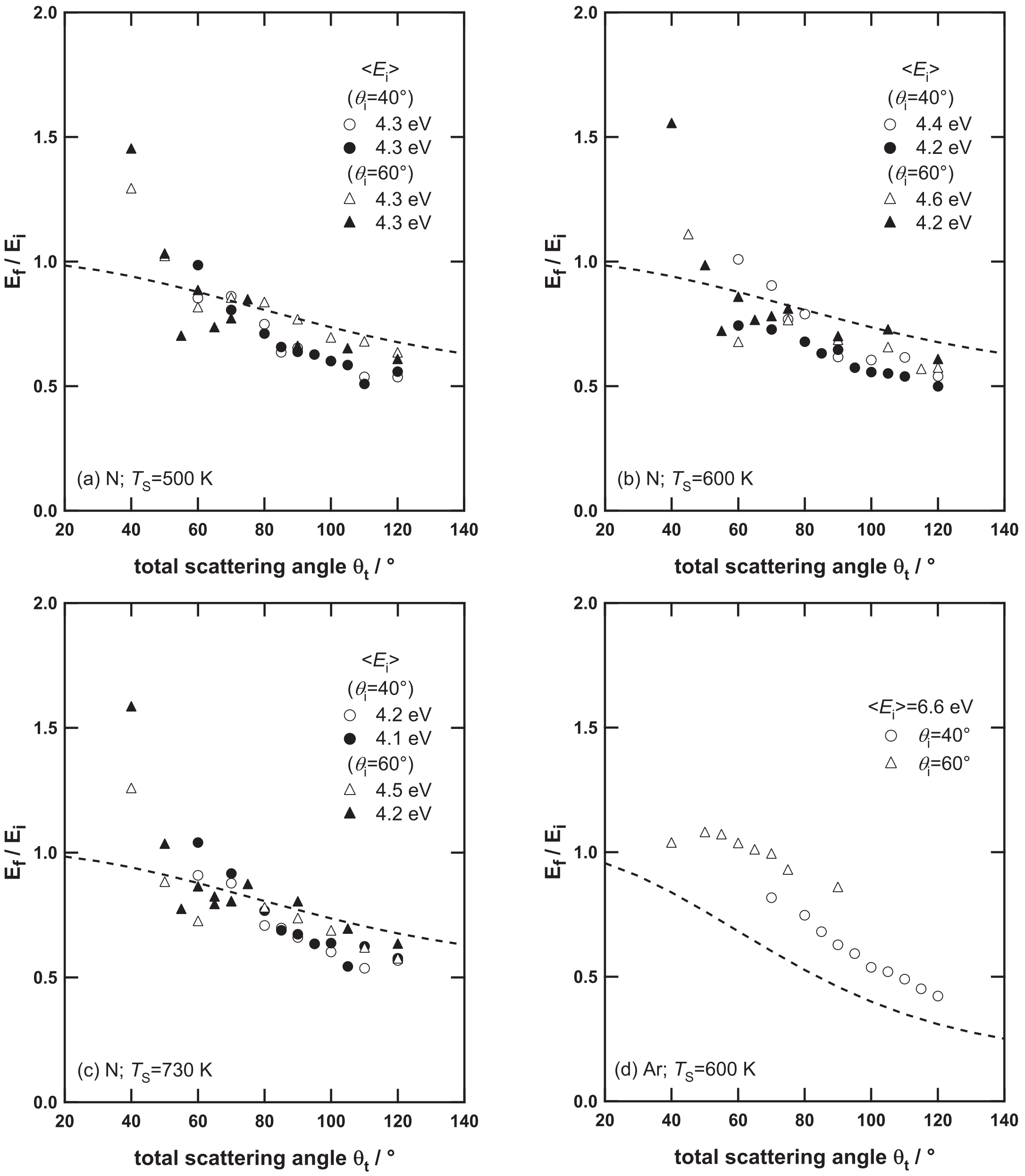

Figure 5. 3 Angle-resolved ratios of final to initial energy (E_f/E_i) plotted as a function of the total scattering angle (θ_t=180-(θ_i+θ_f)) for N atoms (<E_i>~4.3 eV) scattered from Ag(111) at (a) T_S=500 K, (b) T_S=600 K and (c) T_S=730 K. (d) shows E_f/E_i for Ar atoms (<E_i>~6.6 eV) scattered from Ag(111) at T_S=600 K. Data sets are shown for θ_i=40° (circles) and θ_i=60° (triangles). Duplicate determinations (open and filled symbols) are shown for N atom scattering. The dashed lines represent the model of single-collision hard-sphere scattering of the incident atoms from an isolated silver "atom" (mass ratios of m_N/M_{Ag}=14/108 and m_{Ar}/M_{Ag}=40/108, respectively).

The broad component in the N distributions shown in figure 5.1 and 5.2 accounts for the majority of scattered atoms. It is evident that N atoms are also scattered into even smaller outgoing angles, which are not accessible by our detector. In addition, both the broad and the sharp components will extend in the out-of-plane directions. Full 3-D integration would further enhance the integrated area of the broad component relative to the sharp one. Atoms in the sharp component appear to experience a repulsive potential at the surface—a noble atom-like interactions. Conversely, atoms in the broad component are scattered with a substantial loss of memory of their initial momentum, suggestive of an attractive interaction potential.

We now consider the average energy of the scattered particles, as determined from the TOF measurements. The normalised final energies ($<E_f>/<E_i>$) determined for the scattered N and Ar atoms at the different surface temperatures are shown as a function of the total scattering angle (θ_t=180°-($\theta_i+\theta_f$)) in figure 5.3(a-d). In all cases the results obtained at θ_i=40° and θ_i=60° have been combined on the same panel. The final energy of Ar increases with decreasing θ_t (increasing outgoing angle) in a manner that is qualitatively consistent with the binary collision model. Comparing the measured values with a simple binary collision model based on a mass ratio m/M=40/108, illustrates that that both data sets are above the model (less energy is lost than is expected for a single binary collision). Plotted as a function of the total scattering angle, the Ar data points for θ_i=40° and θ_i=60° do not overlap. Ar atoms scattered at θ_i=60° retains significantly more of their initial energy for a given total scattering angle. The θ_i=40° data points are closer to the binary collision model than those determined for θ_i=60°. The behaviour may be indicative of the occurrence of multiple forward collisions that allow atoms to retain more of their initial energy while scattering through a given total scattering angle [54, 55]. In this scenario, Ar incident at θ_i=60° are more likely to experience multiple collisions than Ar atoms incident at θ_i=40°. As a consequence, atoms would lose less energy at θ_i=60° and the energy loss as a function of total scattering angle would be more gradual.

In contrast to Ar, the data points for N at θ_i=40° and θ_i=60° overlap with each other reasonable well when plotted as a function of the θ_t. This implies single collision events or interaction with a more corrugated surface potential than was the case for Ar. In general, the energy ratios determined for θ_i=60° seem to be slightly higher than those for θ_i=40°. This is similar to, but far less pronounced than, the behaviour observed for Ar scattering. Note that, since the scattered N atoms still retain a substantial fraction of their original energy irrespective of the outgoing angle, they do not experience extensive thermalisation at the surface. Hence the broad angular component evident in figure 5.1 and 5.2 does not arise from a prolonged trapping-desorption mechanism at the surface.

The data for N incident at θ_i=60° shown in figure 5.3(a-c) appears to dip consistently at θ_t~60°. This is the specular scattering direction for that incidence angle and corresponds to the maximum of the sharp component seen in figure 5.2. Consequently, it suggests that the atoms scattered into the sharp component tend to lose more energy than the atoms scattered into the broad component. Also for θ_i=60°, there is a dramatic increase in $<E_f>/<E_i>$ as a function of angle at the most grazing outgoing angles ($\theta_f \geq 60°$, $\theta_t \leq 60°$). $<E_f>/<E_i>$ exceeds 1 at the most grazing trajectories (i.e., the average energy of the scattered atoms exceeds that of the incident atoms). The largest values of $<E_f>/<E_i>$ for θ_i=60° occur at total scattering angles that are inaccessible at θ_i=40°. In the θ_i=40° data there is also an increase in $<E_f>/<E_i>$ at the

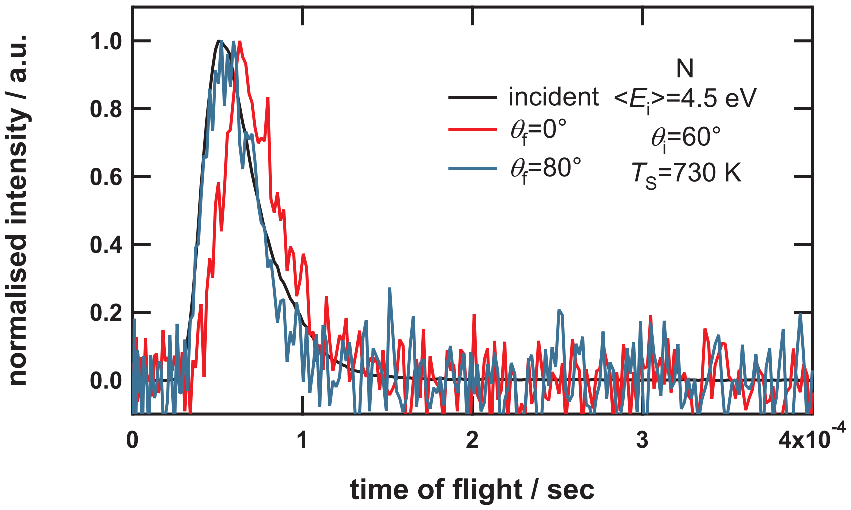

Figure 5. 4 Normalised time-of-flight spectra for the <E_i>=4.6 eV N incident beam (black line) and the resultant spectra, after scattering from Ag(111) at the T_S=730 K surface, for θ_i=60°, θ_f=0 (red line) and θ_i=60°, θ_f=80° (blue line). All spectra have been corrected for the N_2 cracking contribution as outlined in the text.

most grazing angles (θ_f=80°; θ_i=60°). However, this increase is far less pronounced than that observed for θ_i=60°. Given the scatter in the data, it is not possible to state conclusively that the effect is real for the θ_i=40° data set.

It is improbable that <E_f> exceeding <E_i> originates from scattered N atoms solely gaining translational energy from the vibrating surface atoms. Instead, the effect may be attributable to a preferential loss of low-energy atoms from the scattered beam along grazing trajectories. An indication that this is the case can be seen in the comparison of normalised TOF spectra measured at θ_f=0°, θ_f=80° and from the incident beam shown in figure 5.4. At θ_f=80° the TOF distribution is slightly narrower than the incident beam and has less intensity in the low-energy tail. This is in spite of the fact that the θ_f=80° data represents a convolution of the distribution of the incoming beam and that of the scattered particles. A capture mechanism can be proposed that could generate the effect observed. Grazing N atoms may be preferentially captured by the Ag surface (due to the longer time spent in the vicinity of the surface). Captured atoms will be removed from the surface by recombination to N_2 and will thus be lost from the N atom distribution. The observed behaviour of <E_f>/<E_i> will arise if the capture-and-loss processes preferentially remove low energy atoms from the scattered beam. To generate the trends observed in figure 5.3, the capture probability must be angle-dependent, with grazing trajectories being the most likely to experience capture. The comparison between θ_i=40° and θ_i=60° shows that the outgoing angle is not the decisive parameter. For θ_i=40° a significant probability of capture may exist only along the grazing exit trajectories. In contrast, for θ_i=60° low energy atoms may have a high probability of capture on both the incoming and the grazing outgoing trajectories. Thus the largest <E_f>/<E_i> values are obtained for the lowest total scattering angles (those not accessible with the θ_i=40°

beam). The basic idea of the measurement is similar to that employed in a study by Rettner *et al.* [56].

The angle-dependent behaviour of the scattered N is in marked contrast to that of the scattered Ar in terms of both angular distributions and final energies. Most of the N atom data is in apparent good agreement with, though somewhat lower than, the single binary collision model, whereas the Ar data points are significantly above that model. It should be noted in this context that the mass difference between N and Ar by itself favours more efficient energy transfer from Ar to Ag. As mentioned above, it is possible to propose multiple forward collisions to explain the Ar behaviour. In contrast, to explain the features observed in the N atom scattering—greater energy loss (relative to Ar) and a broad (memory-loss) angular distribution—harder and randomising double/multiple collisions would have to be invoked. N atoms should be able to probe the chemisorption potential directly since they encounter no activation barrier and can penetrate closer to the surface atomic cores. In other words, they should indeed see a more corrugated potential energy surface. More multiple collisions would be expected at such a potential surface, resulting in some memory loss of the initial momentum, while nonetheless retaining a relatively high translational energy. As previously reported, this is the nature of nonthermal scattering of reactive particles [28-30].

The two-component distributions, most clearly seen for N scattering at θ_i=60° immediately suggest that there are two relatively distinct scattering processes occurring. Both could, in principle, manifest from a rainbow scattering process [5, 57]. The simplest conceptual explanation is to attribute the sharper component to single-collision scattering from the rainbow scattering region between the Ag surface atoms, while the broader component arises from scattering in regions with a more rapidly varying corrugation. Increasing the surface temperature leads to enhanced surface vibrations. This would typically result in a broadening (intensity reduction) of the rainbow-like sharp component, while the broader component would be largely unperturbed. However, the distributions observed probably do not arise from a rainbow scattering effect, since it would be unusual for a rainbow peak to appear near the specular direction.

Laterally different scattering potentials may be invoked to explain the two-component angular distribution: a physisorption potential, similar to that of Ar, and a deep chemisorption potential. This could imply very rapid local changes of the character of the surface, such as observed for the scattering NO and CO from the H-covered Ru(0001) surface [58-60]. However, in that case the presence of H atoms provides a natural explanation for highly localised changes of the surface potential. In the current system there are no obvious reasons why such localised changes should occur. Instead, the origin of the two-component distributions may lie in the beam rather than on the surface. As mentioned in experimental section, our N beam includes not only ground state N(^{4}S), but also electronically excited (N(^{2}D) and/or N(^{2}P)) states. The different states of N will interact with different potential surfaces. Kokh *et al.* [39] have computed N—Ag_{91} potential energy curves that show a large difference between the potentials of N(^{4}S)+Ag$_{91}$ and N(^{2}D)+Ag$_{91}$ (see figure 1.4 in this thesis). The N(^{2}D)+Ag$_{91}$ potential has a more attractive well than the N(^{4}S)+Ag$_{91}$ potential, the latter being primarily repulsive. Consequently, the scattering behaviour of the different states in our incident beam should differ. Note that Kokh *et al.* believe that their calculation may have underestimated the N-Ag binding energy. Hence the specific potential curves that they show should be considered qualitatively.

Using the potentials calculated by Kokh *et al.*, two extreme cases can be envisaged. In the first case, N(^{4}S) and N(^{2}D) atoms avoid intersystem crossing (spin conversion of N atoms during the interaction are freely permitted) [61, 62]. In this case, N(^{4}S) atoms would transition to the ^{2}D state in the vicinity of the surface and would feel the N(^{2}D)—Ag attractive potential well. Conversely, N(^{2}D) atoms would experience a N(^{4}S)—Ag like repulsive potential. The other extreme case is where intersystem crossing does occur (inter-state transitions are forbidden). This implies the reverse scenario: the ^{2}D state experiences a significant attractive potential while the ^{4}S interacts with a primarily repulsive one.

Considering the cumulative contribution from in- and out-of-plane scattering of N atoms, the broad component of the angular distributions shown in figure 5.1 and 5.2 is clearly dominant. This component is indicative of scattering from an attractive potential, whereas the sharp component suggests a repulsive interaction. As outlined in the experimental section, we believe that the N(^{4}S) atoms represent the largest population in our incident beam. Consequently, the broad component should be attributed to scattering of N(^{4}S) atoms implying that the ^{4}S state must probe an attractive surface potential and that interstate conversion occurs at the surface.

In terms of the two extremes outlined above, the integrated areas of the two scattered components would be representative of the initial composition of the primary beam. However, if the state conversion is not 100% efficient, some N(^{4}S) atoms will still experience a repulsive wall interaction (and some ^{2}D atoms will experience the attractive well). In this case, the relative areas of the scattered components will not be purely indicative of the initial beam composition but will be convoluted with the inter-conversion probabilities at the surface. The relative magnitudes of the two components suggest that spin flipping is likely and that the majority of incident N atoms do experience an attractive well near the surface. These atoms will undergo a potential-induced acceleration at the surface and will have a temporarily increased kinetic energy during the collision with Ag. Consequently, these atoms can be expected to lose more energy (in absolute terms) during a binary collision than atoms that do not experience the attractive interaction. This may account for some of the differences in energy loss behaviour between N and Ar exhibited in figure 5.3.

5.4 Conclusions

The results of N atoms with hyperthermal energy scattering from the Ag(111) surface show that remarkably different behaviour occurs as compared with the physisorption system of Ar/Ag(111). Scattered N atoms have a very large angular spread that contains two components, a broad distribution and a sharp peak. Given their relative masses, N atoms lose energy at the surface more efficiently than Ar atoms. In addition, they experience a loss mechanism at small total scattering angles that preferentially removes low-energy atoms from the beam. The observed behaviour can be explained in terms of a large proportion of the incident N atoms probing a highly corrugated surface due to their interaction with the deep chemisorption potential. The majority of N atoms probably undergo spin-state changes during their interaction with the surface. In contrast, Ar atoms, which interact only with the physisorption potential, scatter from a much flatter surface.

Bibliography

[1] A.W. Kleyn, W. Koppers, N. Lopes Cardozo, Vacuum, **80** (2006) 1098-1106.
[2] A.W. Kleyn, N.J. Lopes Cardozo, U. Samm, Physical Chemistry Chemical Physics, **8** (2006) 1761-1774.
[3] J.A. Barker, D.J. Auerbach, Surface Science Reports, **4** (1984) 1-99.
[4] A.W. Kleyn, Chemical Society Reviews, **32** (2003) 87-95.
[5] A.W. Kleyn, Chapter 2 Basic Mechanisms in Atom-Surface Interactions, in: E. Hasselbrink, B.I. Lundqvist (Eds.) Handbook of Surface Science, Elsevier, Amsterdam, 2008, pp. 29-52.
[6] J.R. Manson, Chapter 3 Energy Transfer to Phonons in Atom and Molecule Collisions with Surfaces, in: E. Hasselbrink, B.I. Lundqvist (Eds.) Handbook of Surface Science, Elsevier, Amsterdam, 2008, pp. 53-93.
[7] S. Roy, N. Shenvi, J.C. Tully, The Journal of Physical Chemistry C, **113** (2009) 16311-16320.
[8] A.M. Wodtke, J.C. Tully, D.J. Auerbach, International Reviews in Physical Chemistry, **23** (2004) 513 - 539.
[9] A. Amirav, M.J. Cardillo, P.L. Trevor, L. Carmay, J.C. Tully, The Journal of Chemical Physics, **87** (1987) 1796-1807.
[10] J.A. Barker, C.T. Rettner, Journal of Chemical Physics, **97** (1992) 5844-5850.
[11] B. Berenbak, S. Zboray, B. Riedmüller, D.C. Papageorgopoulos, S. Stolte, A.W. Kleyn, Physical Chemistry Chemical Physics, **4** (2002) 68-74.
[12] M.D. Ellison, C.M. Matthews, R.N. Zare, The Journal of Chemical Physics, **112** (2000) 1975-1983.
[13] W.J. Hays, W.E. Rodgers, E.L. Knuth, The Journal of Chemical Physics, **56** (1972) 1652-1657.
[14] D. Kulginov, M. Persson, C.T. Rettner, D.S. Bethune, The Journal of Physical Chemistry, **100** (1996) 7919-7927.
[15] R.J.W.E. Lahaye, A.W. Kleyn, S. Stolte, S. Holloway, Surface Science, **338** (1995) 169-182.
[16] E. Pollak, S. Miret-Artés, The Journal of Chemical Physics, **130** (2009) 194710.
[17] A. Raukema, R.J. Dirksen, A.W. Kleyn, The Journal of Chemical Physics, **103** (1995) 6217-6231.
[18] C.T. Rettner, J.A. Barker, D.S. Bethune, Physical Review Letters, **67** (1991) 2183-2186.
[19] H.F. Winters, H. Coufal, C.T. Rettner, D.S. Bethune, Physical Review B, **41** (1990) 6240-6256.

[20] M.J. Romney, J.B. Anderson, The Journal of Chemical Physics, **51** (1969) 2490-2496.
[21] P.S. Weiss, A. Amirav, P.L. Trevor, M.J. Cardillo, Journal of Vacuum Science & Technology a-Vacuum Surfaces and Films, **6** (1988) 889-894.
[22] K.D. Gibson, S.J. Sibener, H.P. Upadhyaya, A.L. Brunsvold, J. Zhang, T.K. Minton, D. Troya, The Journal of Chemical Physics, **128** (2008) 224708.
[23] Y. Watanabe, H. Yamaguchi, M. Hashinokuchi, K. Sawabe, S. Maruyama, Y. Matsumoto, K. Shobatake, Chemical Physics Letters, **413** (2005) 331-334.
[24] Y. Watanabe, H. Yamaguchi, M. Hashinokuchi, K. Sawabe, S. Maruyama, Y. Matsumoto, K. Shobatake, European Physical Journal D, **38** (2006) 103-109.
[25] U. Tasic, D. Troya, Physical Chemistry Chemical Physics, **10** (2008) 5776-5786.
[26] E. Ghio, L. Mattera, C. Salvo, F. Tommasini, U. Valbusa, The Journal of Chemical Physics, **73** (1980) 556-561.
[27] H. Frank, H. Hoinkes, H. Wilsch, Surface Science, **63** (1977) 121-142.
[28] K.P. Giapis, T.A. Moore, T.K. Minton, Journal of Vacuum Science & Technology a-Vacuum Surfaces and Films, **13** (1995) 959-965.
[29] G.S. Hwang, C.M. Anderson, M.J. Gordon, T.A. Moore, T.K. Minton, K.P. Giapis, Physical Review Letters, **77** (1996) 3049-3052.
[30] T.K. Minton, K.P. Giapis, T. Moore, The Journal of Physical Chemistry A, **101** (1997) 6549-6555.
[31] D.J. Garton, T.K. Minton, M. Alagia, N. Balucani, P. Casavecchia, G.G. Volpi, Faraday Discussions, **108** (1997) 387-399.
[32] D.J. Garton, T.K. Minton, M. Alagia, N. Balucani, P. Casavecchia, G.G. Volpi, The Journal of Chemical Physics, **112** (2000) 5975-5984.
[33] D.J. Garton, T.K. Minton, M. Alagia, N. Balucani, P. Casavecchia, G.G. Volpi, The Journal of Chemical Physics, **114** (2001) 5958-5958.
[34] D. Troya, G.C. Schatz, International Reviews in Physical Chemistry, **23** (2004) 341-373.
[35] J. Zhang, D.J. Garton, T.K. Minton, The Journal of Chemical Physics, **117** (2002) 6239-6251.
[36] R.N. Carter, M.J. Murphy, A. Hodgson, Surface Science, **387** (1997) 102-111.
[37] A.C. Kummel, G.O. Sitz, R.N. Zare, J.C. Tully, The Journal of Chemical Physics, **91** (1989) 5793-5801.
[38] G.C. Wang, L. Jiang, X.Y. Pang, J. Nakamura, The Journal of Physical Chemistry B, **109** (2005) 17943-17950.
[39] D.B. Kokh, R.J. Buenker, J.L. Whitten, Surface Science, **600** (2006) 5104-5113.
[40] R.P. Dahiya, M.J. de Graaf, R.J. Severens, H. Swelsen, M.C.M. van de Sanden, D.C. Schram, Physics of Plasmas, **1** (1994) 2086-2095.
[41] S. Mazouffre, I. Bakker, P. Vankan, R. Engeln, D.C. Schram, Plasma Sources Science and Technology, **11** (2002) 439.
[42] A. Raukema, Dynamics of Chemisorption, in, University of Amsterdam, 1995.
[43] F. Gou, M.A. Gleeson, J. Villette, A.W. Kleyn, Vacuum, **81** (2006) 196-201.
[44] M.C.M. van de Sanden, G.M. Janssen, J.M. de Regt, D.C. Schram, J.A.M. van der Mullen, B. van der Sijde, Review of Scientific Instruments, **63** (1992) 3369-3377.
[45] M.C.M. van de Sanden, R.J. Severens, J.W.A.M. Gielen, R.M.J. Paffen, D.C. Schram, Plasma Sources Sci T, **5** (1996) 268-274.
[46] A. Raukema, A.P. de Jongh, H.P. Alberda, R. Boddenberg, F.G. Giskes, E. de Haas, A.W. Kleyn, H. Neerings, R. Schaafsma, H. Veerman, Measurement Science & Technology, **8** (1997) 253-261.

[47] S.N. Foner, R.L. Hudson, The Journal of Chemical Physics, **37** (1962) 1662-1667.
[48] C.-L. Lin, F. Kaufman, The Journal of Chemical Physics, **55** (1971) 3760-3770.
[49] M. Alagia, V. Aquilanti, D. Ascenzi, N. Balucani, D. Cappelletti, L. Cartechini, P. Casavecchia, F. Pirani, G. Sanchini, G.G. Volpi, Israel Journal of Chemistry, **37** (1997) 329-342.
[50] B. Brunetti, G. Liuti, F. Pirani, E. Luzzatti, Chemical Physics Letters, **84** (1981) 201-204.
[51] K.C. Janda, J.E. Hurst, C.A. Becker, J.P. Cowin, D.J. Auerbach, L. Wharton, The Journal of Chemical Physics, **72** (1980) 2403-2410.
[52] M.E.M. Spruit, E.W. Kuipers, F.H. Geuzebroek, A.W. Kleyn, Surface Science, **215** (1989) 421-436.
[53] S.K. So, R. Franchy, W. Ho, The Journal of Chemical Physics, **91** (1989) 5701-5706.
[54] H.H. Brongersma, M. Draxler, M. de Ridder, P. Bauer, Surface Science Reports, **62** (2007) 63-109.
[55] H. Niehus, W. Heiland, E. Taglauer, Surface Science Reports, **17** (1993) 213-303.
[56] C.T. Rettner, H.A. Michelsen, D.J. Auerbach, Chemical Physics, **175** (1993) 157-169.
[57] A.W. Kleyn, T.C.M. Horn, Physics Reports-Review Section of Physics Letters, **199** (1991) 191-230.
[58] B. Berenbak, B. Riedmüller, S. Stolte, A.W. Kleyn, Chemical Physics, **301** (2004) 309-313.
[59] D.A. Butler, B. Berenbak, S. Stolte, A.W. Kleyn, Physical Review Letters, **78** (1997) 4653-4656.
[60] B. Riedmüller, I.M. Ciobîca, D.C. Papageorgopoulos, B. Berenbak, R.A. van Santen, A.W. Kleyn, Surface Science, **465** (2000) 347-360.
[61] J.W. Gadzuk, Physical Review Letters, **76** (1996) 4234-4237.
[62] J.W. Gadzuk, J.K. Nørskov, The Journal of Chemical Physics, **81** (1984) 2828-2838.